RESEARCH ARTICLE

National Science Open
4: 20240014, 2025
https://doi.org/10.1360/nso/20240014

Engineering

Special Topic: Flexible Electronics and Micro/Nanomanufacturing

Calibration-free estimation algorithm for cuffless continuous blood pressure measurement based on ultrasonic devices

Jiarui Tang[1,#], Haotian Lei[1,#], Tianyu Kang[1,#], Zihao Wang[2,#], Yang Yu[1], Ye Tian[1], Yixuan Wang[2], Hanchuan Tang[1,*], Nianguo Dong[2,*] & Jianfeng Zang[1,3,*]

[1]*School of Integrated Circuits and Wuhan National Laboratory for Optoelectronics, Huazhong University of Science and Technology, Wuhan 430074, China;*
[2]*Thoracic and Cardiovascular Surgery, Union Medical College Hospital, Tongji Medical College, Huazhong University of Science and Technology, Wuhan 430074, China;*
[3]*The State Key Laboratory of Intelligent Manufacturing Equipment and Technology, Huazhong University of Science and Technology, Wuhan 430074, China*

#Contributed equally to this work.
*Corresponding authors (emails: jfzang@hust.edu.cn (Jianfeng Zang); 1986XH0694@hust.edu.cn (Nianguo Dong); hctang1@hust.edu.cn (Hanchuan Tang))

Received 29 April 2024; Revised 2 July 2024; Accepted 30 July 2024; Published online 31 July 2024

Abstract: The rising global impact of hypertension calls for innovative approaches to achieve accurate and continuous blood pressure monitoring. Traditional cuff-based methods and pulse-transit-time (PTT) measurements face challenges, including discontinuity and the need for frequent calibration. Here, we introduce a paradigm-shifting method using a flexible ultrasonic array for calibration-free estimation. The conformal ultrasonic device, which integrates piezoelectric composites, copper electrodes, and a stretchable Polydimethylsiloxane substrate, precisely measures the radial artery diameter with an error margin controlled within 3%. The calibration-free algorithm, based on the Powalowski and Pensko model, establishes a dynamic correlation between arterial blood pressure and vessel diameter, with estimation errors within 1.2 ± 1.0 mmHg. Long-term monitoring over 30-day showcased the model's stability. Our approach eliminates the need for frequent calibration, enhances accuracy, and offers a comprehensive insight into the dynamic relationship between blood pressure and vessel diameter. This innovation holds promise for revolutionizing continuous blood pressure monitoring, contributing to early detection and intervention in hypertensive individuals.

Keywords: blood pressure measurement, calibration-free, wearable ultrasonic devices, flexible electronics

INTRODUCTION

Hypertension is a major global health issue, contributing to over 8.5 million deaths annually. It is a leading risk factor for conditions such as stroke, ischemic heart disease, vascular diseases, and kidney diseases. Recent research [1] reveals a worrisome trend: over the last three decades, the number of hypertensive adults aged 30–79 has surged from 650 million to 1.28 billion, with almost half of them unaware of their condition. The World Health Organization underscores the importance of early detection and intervention in hypertension, achievable through regular blood pressure monitoring, either at home or in a medical setting. This

approach facilitates initial blood pressure control through lifestyle interventions. Although traditional cuff blood pressure (BP) devices offer regular monitoring, they suffer from discontinuity and cannot provide prolonged daily blood pressure monitoring. Therefore, investigating novel methods for continuous blood pressure monitoring is crucial for diagnosis and prevention.

Currently, continuous blood pressure measurement is achievable through the invasive method of catheterization, which remains the gold standard. This method uses a strain gauge to measure blood pressure at any arterial site. Other blood pressure measurements are taken intermittently, with longer intervals [2]. These non-invasive methods primarily require an inflatable cuff [3]. Several methods have emerged to measure blood pressure without the use of a cuff, often employing electrocardiogram (ECG) and photoplethysmogram (PPG) signals to estimate pulse transit time (PTT). Combined with the Moens-Korteweg formula, these methods calculate blood pressure [4–8]. Some studies have advanced by integrating additional physiological parameters with PTT, producing more comprehensive blood pressure estimation models [9–13], yielding promising results. However, despite the benefits of PTT-based techniques, they encounter challenges, such as the need for multiple sensors, increasing hardware expenses, and potential inconvenience. Moreover, Systematic errors often arise in PTT-based measurement methods due to inaccurate estimation of pulse propagation distance, leading to significant inaccuracies and the need for frequent calibration. Consequently, these limitations impede the widespread acceptance of PTT-based techniques for blood pressure measurement.

A promising alternative for blood pressure estimation is the ultrasound-based method [14–18]. Unlike other methods, ultrasound exhibits strong penetrability, reaching depths of more than 4 cm in human tissue. With a single sensor, it can monitor the blood vessel diameter waveform to accurately estimate the blood pressure waveform. However, the current ultrasonic blood pressure estimation model primarily relies on an analytical model based on a single parameter of vascular cross-sectional area. This model has limitations as it fails to consider essential physiological parameters influencing blood pressure. In addition, the linear calibration method mainly used in the model requires frequent calibration, which reduces its reliability. Some nonlinear calibration methods, such as Gao's nonlinear arterial load model, are expensive to calculate and cannot estimate blood pressure in real time [19]. Huynh's IPG-based model requires additional sensors to be worn [20].

This paper introduces a novel technique employing a flexible ultrasonic array to measure the radial artery of the wrist. This approach extracts physiological characteristics like vessel diameter and waveform, which are fused to establish a multi-dimensional regression model based on Support Vector Regression (SVR). The resulting model has demonstrated excellent long-term predictive capabilities for blood pressure in experiments.

By leveraging the flexibility of the ultrasonic array, this innovative approach accurately measures the radial artery, providing critical insights into physiological characteristics essential for predicting blood pressure. The fusion of vessel diameter and waveform features yields a multi-dimensional regression model based on SVR, showcasing excellent predictive capabilities in long-term experiments.

The remainder of this paper is organized as follows. Firstly, we will detail the hardware and experimental methods of ultrasonic measurement. Secondly, we will introduce the proposed method. Thirdly, we will present the experimental results. At last, we will demonstrate the results and compare them with other works, whileconcluding the paper.

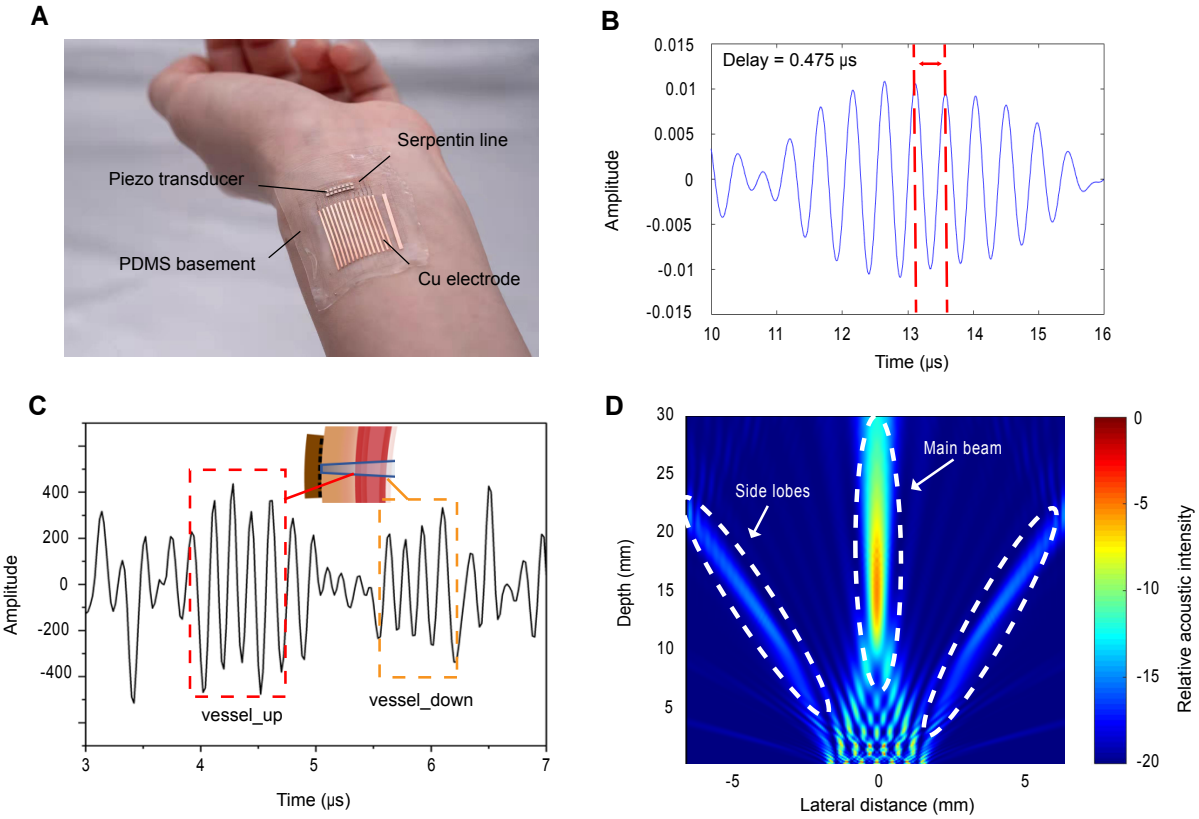

Figure 1 Working principle of ultrasonic measurement of blood vessel diameter. (A) Wearing a schematic diagram of the flexible ultrasonic array, which includes four parts: Piezo transducer, serpentine line, PDMS basement, and Cu electrode. (B) At a 2 MHz frequency, the ultrasonic wavelength is about 0.69 mm. It has both good bandwidth (yellow line) and signal quality. (C) A single pulse in the upper and lower walls of arteries will produce a high energy echo due to the difference in acoustic impedance, and then the ultrasonic sensor as the echo receiver receives the echo and converts it into a high level of electrical signal. (D) The array is set to seven ultrasonic arrays of 0.9 mm length and spacing, and excited at a center frequency of 7.5 MHz.

MATERIALS AND METHODS

Data collection and hardware

The conformal ultrasonic device comprises several integral components, namely piezoelectric composites, copper electrodes, serpentine wires facilitating stretchable connections, and a Polydimethylsiloxane (PDMS) soft material substrate specifically engineered for wearable measurements (as depicted in Figure 1A). After our test, we chose an array structure with an array size of 300 μm, array spacing of 100 μm, and array element number of 2*7. This structure ensures that the main lobe width of the ultrasonic beam is narrow, the energy is concentrated, and the sidelobe is minimized. They emit and receive ultrasonic echoes with a central frequency of 10 MHz, autonomously detected without external triggering. Figure 1B shows the axial resolution of the 7.5 MHz ultrasonic transducer with a delay of 0.475 μs and a calculated half-peak width of about 0.21 mm. The minimum measured vessel diameter is about 0.2 mm, and changes in the diameter of the radial artery can be keenly monitored. The resulting echo signal is portrayed in Figure 1C, which shows two peaks corresponding to the anterior and posterior walls of the radial artery. The radial artery's diameter can be precisely calculated by assessing the variance in peak values. This plot unveils a center frequency of

7.5 MHz, a wavelength of 0.21 mm, and a peak-to-peak voltage of approximately 200 mV. The array is set to seven ultrasonic arrays of 0.9 mm length and spacing, and excited at a center frequency of 7.5 MHz. The sound field simulation results are shown in the Figure 1D.

The ultrasonic device, owing to its flexible and conformal design, exhibits commendable stretchability, contributing to a heightened signal-to-noise ratio. Consequently, it attains accurate and reliable measurements of blood vessel diameters. Additionally, this stretchable design ensures the device's stability during prolonged monitoring, sustaining the accuracy and consistency of measurements.

Calibration-free BP estimation algorithm

In the cardiac cycle of the human body, alterations in human blood pressure lead to periodic changes in the diameter of blood vessels. Notably, a discernible correlation exists between human blood pressure and blood vessel diameter. The blood vessel wall is composed three distinct layers: the inner membrane, the middle membrane, and the outer membrane. The inner membrane, characterized by extreme thinness and smoothness, serves to minimize resistance to blood flow within the vessels. Meanwhile, the middle membrane, consisting of muscle cells, represents the thickest of the three layers. This muscular layer imparts substantial elasticity to facilitate the expansion and contraction of blood vessels. Lastly, the outer membrane, composed of connective tissue, plays a vital role in furnishing nutrients to the blood vessels.

The intricate, multilayered structure induces complex nonlinear viscoelastic behavior in human blood vessels when subjected to external forces [21]. Consequently, comprehending the relationship between arterial blood pressure and blood vessel diameter is of paramount importance. This relationship fundamentally determines the precision of measured blood pressure values.

Numerous researchers have conducted investigations to elucidate the relationship between arterial blood pressure and blood vessel diameter. Scholars have unveiled a robust exponential correlation between these variables, as encapsulated in the model formulated by Powalowski and Pensko [22]. This correlation is mathematically represented as follows:

$$P(t) = p_0 e^{\beta A(t)} \tag{1}$$

Within this formula, p_0 and β can be regarded as constants. Moreover, if systolic and diastolic blood pressures are denoted as p_s and p_d respectively, and the cross-sectional areas of blood vessels are denoted as A_s and A_d, then p_0 can be expressed in terms of diastolic blood pressure:

$$p_0 = \frac{p_d}{e^{\beta A_d}} \tag{2}$$

Substituting Equation 2 into Equation 1 yields:

$$p(t) = p_d e^{\frac{\beta}{A_d}\left(\frac{A_d}{A(t)}-1\right)} \tag{3}$$

Let $\alpha = \beta/A_d$, then Equation 3 can be reformulated as:

$$p(t) = p_d e^{\alpha\left(\frac{A(t)}{A_d}-1\right)} \tag{4}$$

To estimate blood pressure within this model, the initial step involves calculating the constant α, expressed as:

$$\alpha = \frac{A_d \ln(p_s / p_d)}{A_s - A_d} \tag{5}$$

The constant α serves as a parameter characterizing the rigidity of blood vessel walls. Previous medical investigations have demonstrated that an individual's sex, age, health, and the type of blood vessels examined influence the value of α [23,24]. Consequently, α can be perceived as the parameter embodying individual differences within the model.

Hence, before employing the aforementioned model, it becomes imperative to measure the values of p_s, p_d, A_s, and A_d. Subsequently, the calculation of the α value, as per Equation 5, becomes essential. This process is tantamount to refining the blood pressure estimation model.

In this model, the parameters α are considered constants and necessitate calibration only during the initial test. Nevertheless, over prolonged monitoring periods, test inaccuracies are prone to escalation, likely stemming from the temporal alteration of the α parameter. Consequently, blood pressure estimation methods utilizing this model confront a trade-off between enduring escalating errors in extended monitoring or requiring recurrent calibration of the α parameter through alternative blood pressure measurement techniques.

To enable sustained blood pressure monitoring over extended periods, a novel calibration-free monitoring method is introduced, as depicted in Figure 2A. In this monitoring approach, data regarding the vascular diameter of the radial artery in the human wrist are initially captured using an ultrasound array. The cross-sectional area of blood vessels can then be computed by incorporating this data into Equation 4. Simultaneously, given that the characteristics of resistance waveforms in peripheral arterial vascular pulse waves are inherently linked to the rigidity of blood vessel walls in medical contexts, characteristic values of vascular pulse waves can be extracted. These values are subsequently employed to formulate a prediction model for the α parameters, which characterize the rigidity of blood vessel walls.

Ultimately, blood pressure estimation is executed using Equation 4, with the incorporation of the calibrated α parameter. This innovative approach facilitates calibration-free blood pressure estimation during prolonged monitoring periods.

Before signal feature extraction, a preprocessing block is implemented to address noise and artifacts present in the original signal, as illustrated in Figure 2B. The primary sources of noise in the original signal encompass baseband drift, electromyographic (EMG) interference, power frequency noise, and other interference.

Baseline drift: One of the principal noises in the diameter pulse wave signal is baseline drift, primarily attributed to the patient's breathing and the movement of the ultrasonic sensor. Typically characterized by a sinusoidal curve with slow transformation and a frequency lower than 1Hz, baseline drift is mitigated using a low-pass Finite Impulse Response (FIR) filter. The FIR filter is selected for its characteristic of no cumulative error and optimal real-time performance.

EMG interference: Irregular high-frequency electrical interference induced by human muscle tremors results in EMG interference. With a broad frequency range typically between 10 to 1000 Hz, this interference manifests as irregular and rapidly changing waveforms. The low-pass filter is applied to eliminate the high-frequency EMG interference signal.

Power frequency noise: Arising from power frequency supply and electromagnetic fields in the device's environment, power frequency noise exhibits periodic small ripples at frequencies of 50 Hz or 60 Hz. A 50 Hz band stop filter is employed to eliminate power frequency noise.

By addressing these noise sources through targeted filtering techniques, the preprocessing stage aims to

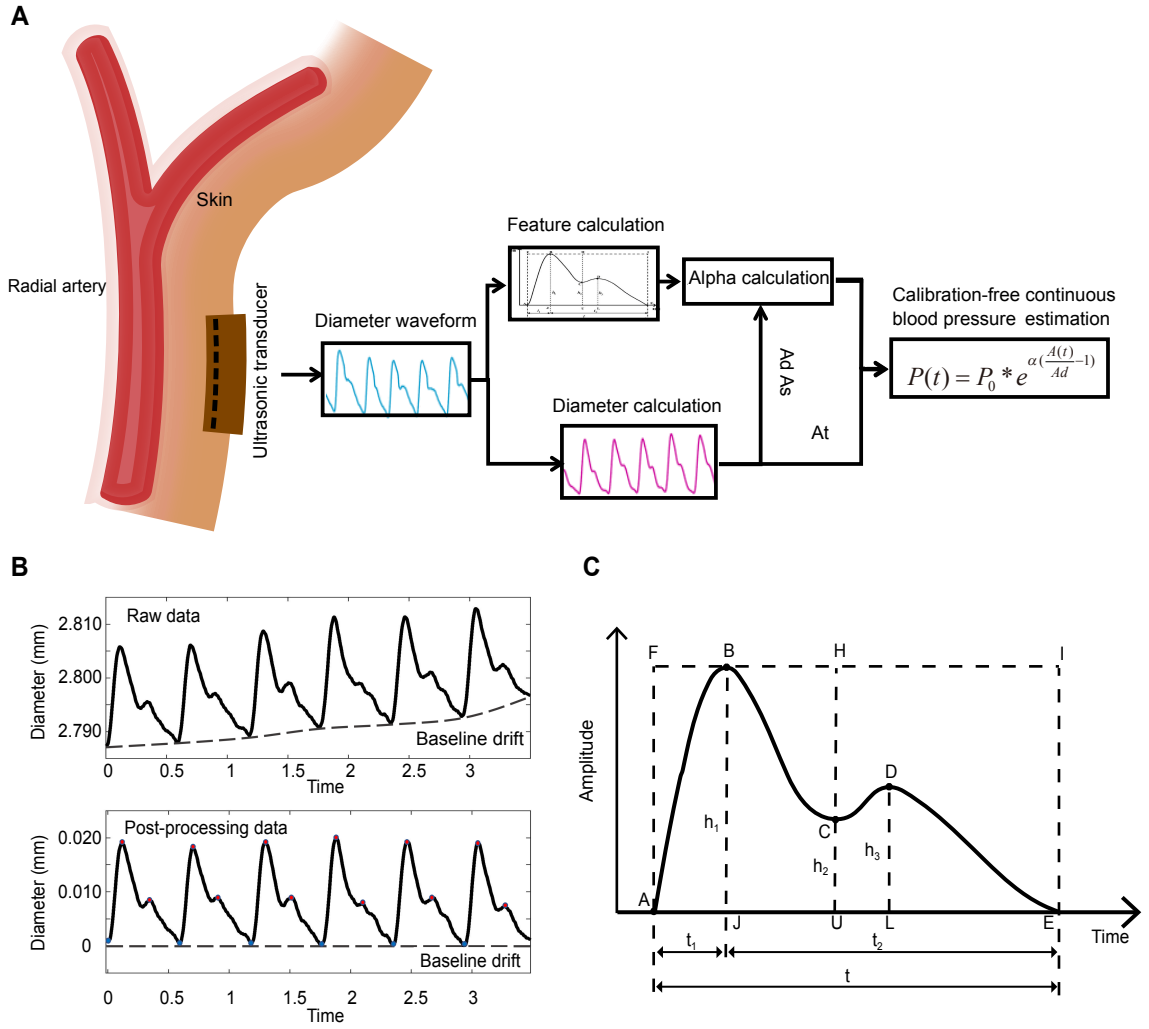

Figure 2 Waveform processing. (A) Block diagram of the proposed BP estimation approach. (B) Vascular pulse wave data preprocessing process. (C) Waveform segmentation and eigenvalue extraction.

enhance the quality of the arterial diameter data for subsequent signal feature extraction.

To enhance the precision of the blood pressure model and facilitate a more accurate estimation of the population-specific parameter, α, this study extracts informative and structural parameters from the blood vessel diameter pulse wave signal, treating them as signal eigenvalues. Informative parameters encapsulate the holistic characteristics of the entire signal, while structural parameters denote characteristics calculated from key points with special physical significance in each pulse cycle.

(a) Informative parameters

Informative parameters encompass features devoid of apparent structural characteristics in the signal. In this study, time-domain features of the overall signal are utilized to construct the model.

(1) Statistical characteristics

The mean value and standard deviation of the diameter signal are considered.

(2) Time domain parameters

Two features are extracted from the time domain: Systolic Cross-Sectional Area (A_s) and Diastolic Cross-

Table 1 Parameter definition and calculation formula

Features	Equations	Definitions
HR	$60/t$	Time span between two main peaks of the wave
T_1	t_1/t	Time span rate between A and J
T_2	t_2/t	Time span rate between J and E
T_{bc}	t_{bc}/t	Time span rate between B and C
T_{cd}	t_{cd}/t	Time span rate between C and D
H_1	h_2/h_1	Relative height of the secondary trough
H_2	h_3/h_1	Relative height of the secondary peak
K_0	S_{ABCE}/S_{AFIE}	Proportion of overall wave area
K_1	S_{ABCU}/S_{AFHE}	Proportion of first peak wave area
K_2	S_{UCDE}/S_{UHIE}	Proportion of second peak wave area
SV	$sin\alpha \sum_{j=s}^{d} Q(t_j)$	Average blood flow during the pulse cycle
MD	MD	Mean value of the wave
SD	SD	Standard deviation of wave
WE	$\sum_{i=1}^{n} p_i \log(p_i)$	Wavelet entropy

Differential parameters that characterize the elasticity of the blood vessel wall in the human body, denoted as α, exhibit slow changes over an extended period. Additionally, external factors such as the intake of antihypertensive drugs can induce alterations in the parameter α. These changes contribute to an escalation in the error of the fundamental blood pressure calculation model. Consequently, many measurement methods necessitate the regular calibration of model parameters using a cuff sphygmomanometer.

Sectional Area (A_d). As per Equation 5, when the valley of diastolic blood pressure and the peak of systolic blood pressure remain constant, A_s and A_d are inversely proportional to the parameter α.

(3) Other parameters

This category includes Wavelet Entropy (WE), representing the degree of signal chaos, and Heart Rate (HR), capturing crucial frequency domain information from the human pulse wave. The formula for calculating wavelet entropy is given as:

$$Hw(p) = -\sum_{i=1}^{n} p_i \log(p_i) \tag{6}$$

(b) Structural parameters

The pulse wave is typically defined by four characteristic points, illustrated in Figure 2C. Point A designates the opening of the aortic valve, reflecting the pressure and volume in the blood vessel post-contraction. Point B represents the highest systolic pressure, indicating the peak of the main wave. Point C marks the initiation of the anti-tide wave and the trough of the robust beat wave. Point D, a double-beat wave, offers insights into the functional status, vascular elasticity, and blood flow of the aortic valve. Finally, Point E denotes the termination of the pulse wave. These distinct points signify various states of the cardiovascular system, holding significant implications for blood pressure calculation models.

Various structural parameters can be derived based on these feature points. Refer to Table 1 for a comprehensive elucidation of the extracted features, encompassing detailed explanations and calculation methodologies.

This study employs characteristic parameters extracted from the pulse wave of blood vessel diameter to model and estimate α. This approach enables real-time calculation and measurement of α, eliminating the need for cumbersome regular measurements.

Following the identification of characteristic parameters, two multivariate analysis methods, namely multiple linear regression (MLR) and support vector regression (SVR), were employed to construct the α calculation model.

The multiple linear regression method, a foundational regression analysis technique, boasts low computational complexity and is resistant to overfitting. Widely applied in multivariate regression prediction scenarios characterized by a robust linear relationship, it expresses the association between α and eigenvalues as follows:

$$\alpha = \beta_0 + \beta_1 f_1 + \beta_2 f_2 + ... + \beta_n f_n \tag{7}$$

The coefficient matrix for each eigenvalue can be computed by minimizing the objective cost function:

$$Q(\beta_0, \beta_1, ..., \beta_n) = \sum_{i=1}^{n} (\alpha - \beta_0 - \beta_1 f_1 - ... - \beta_n f_n)^2 \tag{8}$$

$$\beta = (X_f^T X_f)^{-1} X_f^T \alpha \tag{9}$$

The support vector machine, a specific algorithm applicable to both classification and regression, utilizes a kernel to capture nonlinear relationships. It demonstrates robust resistance to noise in the data. Leveraging its superior regression prediction capabilities for nonlinear relationships in the model, a Gaussian radial basis function kernel (RBF kernel) is employed for regression analysis.

$$K(x, z) = \exp(-\frac{x - z^2}{2\sigma^2}) \tag{10}$$

RESULTS

Experimental protocol

In this investigation, our primary objective was to formulate a calibration-free model for estimating blood pressure, utilizing a test cohort comprising 50 volunteers. The cohort comprised 34 men and 16 women, with an average age of 24 ± 1.2 years. The experimental protocol consists of three test categories: (1) reference blood pressure (BP) measurement, (2) commercial ultrasonic measurement, and (3) flexible ultrasonic estimation.

For the reference BP measurement, participants maintained a seated position while an electronic sphygmomanometer (OMRON J732) cuff was applied to their left upper arm at heart level. Blood pressure was recorded three consecutive times, and the average of these readings constituted the reference BP. In the case of commercial ultrasonic measurement, participants, in a seated position, underwent measurement of the radial artery in their left wrist using commercial ultrasound. The resulting data were stored and extracted for use as reference data. Subsequently, flexible ultrasound arrays were affixed to the radial artery of the wrist for flexible ultrasonic estimation. Real-time measurement and transmission of radial artery diameter information to a computer were executed for display and storage. These systematic experiments led to the development of a calibration-free model for blood pressure estimation. Our proposed model stands to streamline and enhance the blood pressure measurement process, holding significant implications for clinical practice. The testing sessions were distributed across three periods: morning, afternoon, and evening. Each test, conducted with the subjects in a seated position, lasted half a minute, and three consecutive tests were performed. Following

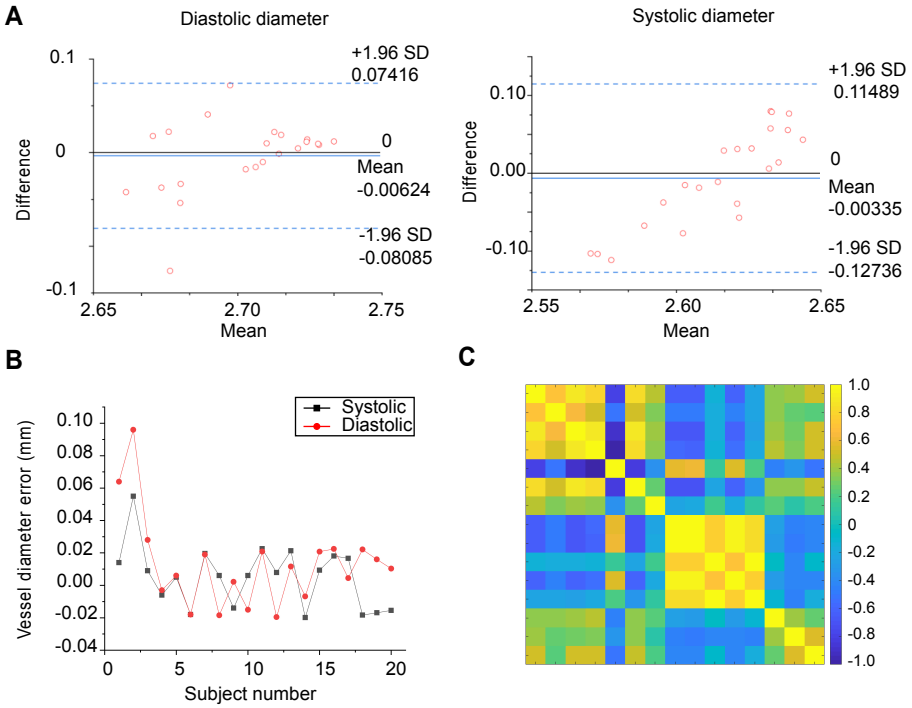

Figure 3 Measurement of vessel diameter and feature selection results. (A) Bland-Altman diagram of systolic and diastolic vessel diameter error (n=22). (B) Diameter measurement error across different individuals (n=20). (C) Pearson correlation matrix, where the parameters are SBP, DBP, HR, T_1, T_2, Tac, Tcd, H_1, H_2, K_0, K_1, K_2, MD, SD, WE, from top to bottom and left to right.

the static test, subjects engaged in 3 sets of 15 squats, with a 30-second rest before resuming the seated test position. The mean systolic blood pressure for all participants was 114.88 ± 16.04 mmHg and 132.98 ± 19.81 mmHg in the morning and evening, respectively. Specifically, the raw data from the first day of each subject served as the model′s training set, while the data from the last three days constituted the test set.

Precision in vessel diameter measurement and feature selection results

Accurate and stable measurement of blood vessel diameter is imperative for ensuring the robustness of our study. Our primary focus in this investigation is to evaluate the precision of wrist radial artery diameter measurement using flexible ultrasound devices. To achieve this objective, we utilized a state-of-the-art all-digital ultrasound imaging diagnostic instrument (Stork) as the standard for diameter measurement.

The study involved obtaining multiple measurements of radial artery diameters across a diverse group of individuals, followed by a meticulous comparative analysis of measurement errors between the two techniques. After testing twenty-two people, our findings clearly illustrate that measurement errors can be effectively controlled within 8 mmHg (3%), as depicted in Figure 3A.

Moreover, variations in diameter measurement errors among different populations are evident (Figure 3B). However, these errors can be effectively controlled to below 20 μm, underscoring the accuracy of the flexible ultrasonic device in vascular diameter measurement.

The examination of test data allows for the computation of the Pearson correlation coefficient between the characteristic parameters and both the target value and among the characteristic parameters. The resulting

Table 2 Selected features for randomly selected subjects

Features	Correlation coefficient	P-value	Definitions
HR	0.88	8.92×10^{-24}	Time span between two main peaks of the wave
T_1	0.80	1.03×10^{-16}	Time span rate between A and J
T_{cd}	0.46	6.21×10^{-05}	Time span rate between C and D
H_1	−0.63	5.02×10^{-09}	Relative height of the secondary trough
SV	0.68	6.51×10^{-11}	Average blood flow during pulse cycle

correlation coefficient matrix is visually represented in Figure 3C.

Evaluation of feature subsets commonly involves assessing criteria such as high correlation between feature parameters and the target, while maintaining low correlation among individual features. In alignment with these standards, the appropriate feature subset can be identified based on the Pearson correlation coefficient matrix. The ultimately selected feature parameters are outlined in Table 2.

Accuracy performance of the model

In this section, the accuracy performance of the established model is shown respectively from three aspects: alpha estimation error, population error, and long-term monitoring results (as depicted in Figure 4A).

Figure 4B illustrates Bland–Altman plots representing systolic (SBP) and diastolic (DBP) blood pressure targets in the test set (The number of test sets is 103). The error in diastolic arterial pressure and systolic arterial pressure is 0.07 ± 4.26 mmHg and 2.42 ± 2.45 mmHg, respectively, indicating compliance with the Association for the Advancement of Medical Instrumentation criteria. These criteria necessitate mean error and standard deviation values to be below 5 mmHg and 8 mmHg, respectively.

Monitoring capability of calibration-free model

In Figure 5A, we evaluated the predictive efficacy of a specific model for estimating blood pressure in a cohort of 50 individuals. The study specifically assessed participants' ability to predict mean error within seven days, focusing on the proportion of individuals maintaining a prediction error below a specified threshold. Results revealed that a significant majority (80%) successfully predicted a mean error of less than 8 mmHg, highlighting the model's robustness across diverse populations. Moreover, almost half of the participants (47.5%) sustained a prediction error below 5 mmHg, underscoring the model's effectiveness in precise blood pressure estimation. These findings suggest the model′s potential as a reliable tool for predicting blood pressure in various individuals.

Ensuring the stability and precision of continuous blood pressure monitoring over extended periods, without the need for calibration with external blood pressure monitors, is pivotal in establishing the calibration-free nature of the model.

In Figure 5B, blood pressure estimation data were collected through month-long monitoring of blood pressure in three subjects. Cuff blood pressure measurements and flexible ultrasound detection system measurements were conducted on days 1, 2, 3, 5, 8, 10, 15, and 30 following the initiation of the test. The data from day 1 served as the training set, extracting feature parameters and completing blood pressure estimation models. Parameter α was recalculated daily based on the multi-feature estimation model. Figure 5B illus-

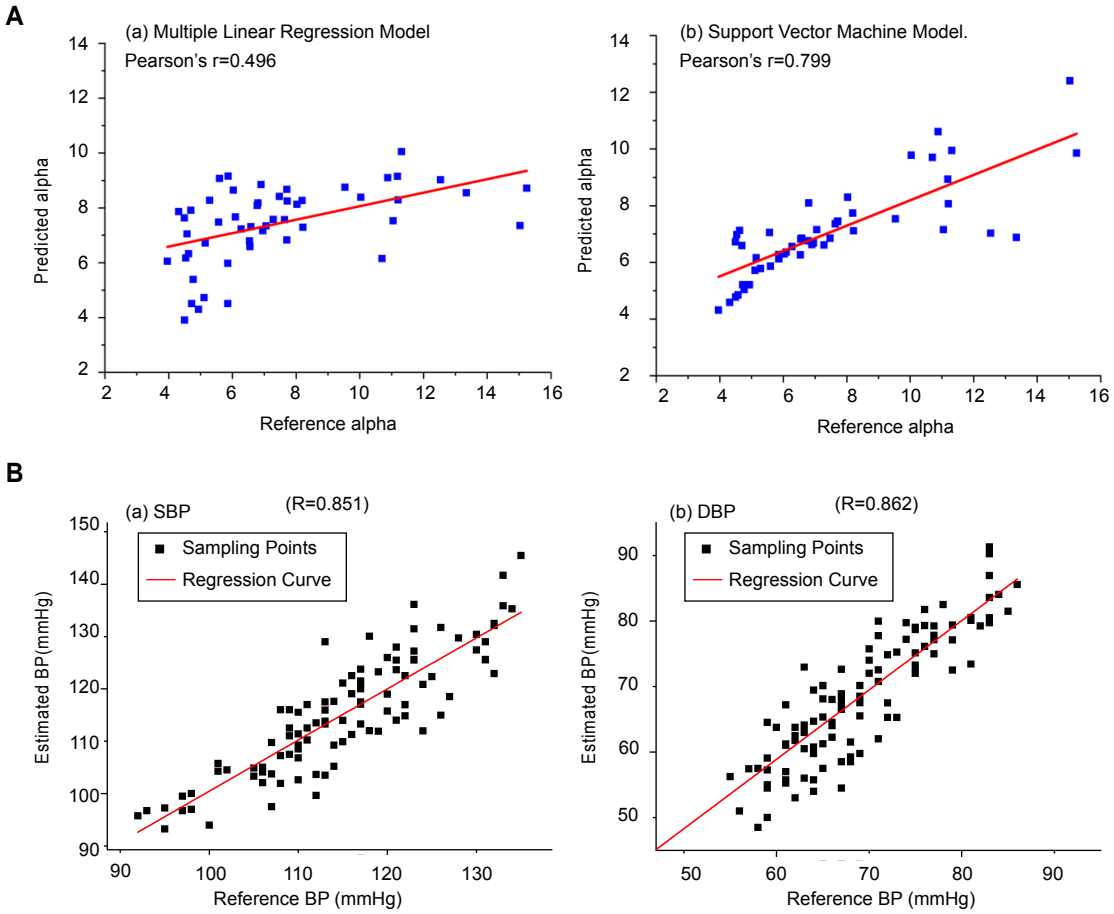

Figure 4 Precision performance and error analysis of the model. (A) Correlation and Bland-Altman plots of alpha predicted value with reference value under multiple linear regression model and support vector machine model. (B) Bland-Altman plot for SBP and DBP.

trates the analysis of the stability results in long-term monitoring of systolic and diastolic blood pressure using the calibration-free blood pressure estimation model.

In Figure 5B, a notable surge in model error is evident from day 3 during the 30 days of long-term monitoring. However, a substantial decrease in error is observed from day 5 to day 8 and after day 15. These findings suggest that the relationship between the blood pressure estimates of the proposed monitoring model and reference blood pressure values fluctuates randomly over time, yet this is unrelated to model degradation during extended monitoring. These error fluctuations may stem from uncontrolled experimental conditions, such as measurement bias in commercial cuff blood pressure monitors, rather than a deterioration of errors in the proposed method over prolonged monitoring.

For instance, the documentation of the Omron sphygmomanometer used as a reference indicates a bias in blood pressure measurements of plus or minus 3 mmHg. The results of the 30-day long-term monitoring affirm the model's effectiveness in providing valid blood pressure estimates over extended periods without the need for calibration of model parameters using a cuffed sphygmomanometer.

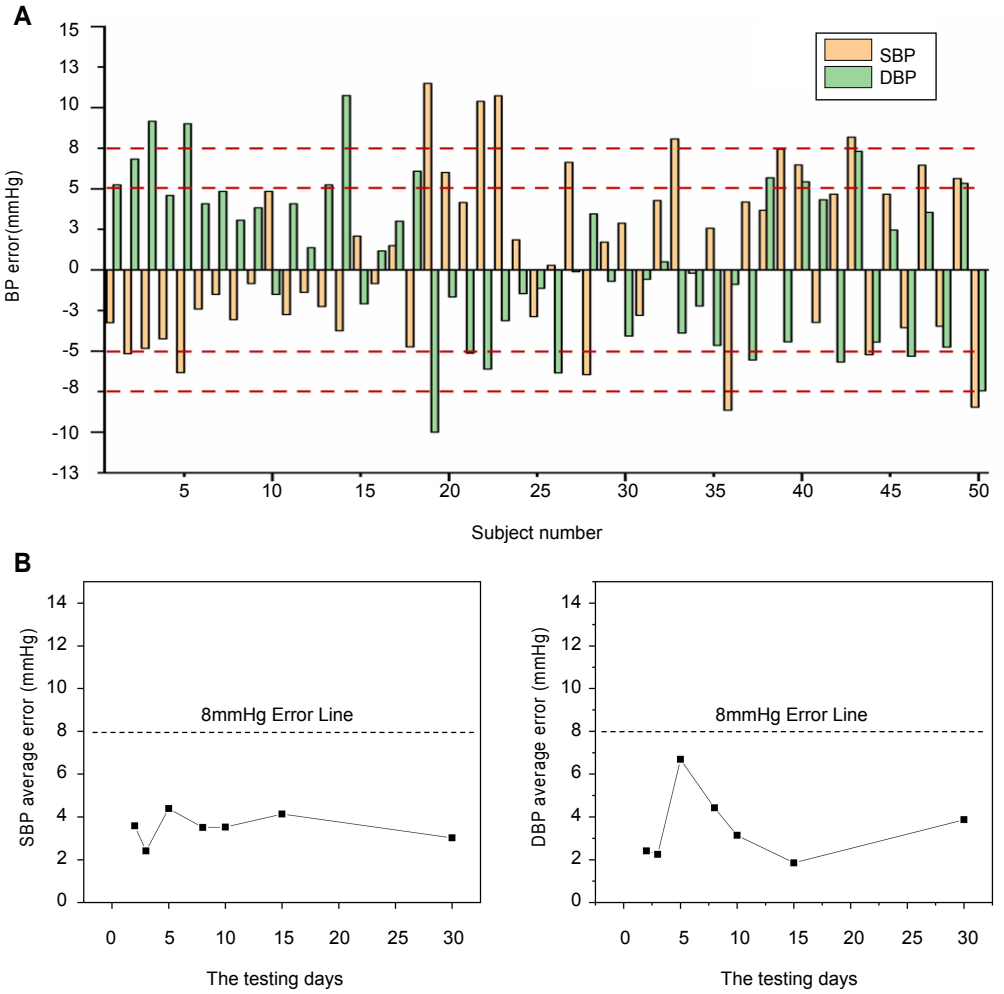

Figure 5 (A) Analysis of blood pressure measurement errors in diverse populations. (B) 30 days long-term systolic and diastolic blood pressure error curve over time.

DISCUSSION

Comparison with other studies

Our proposed blood pressure monitoring method presents substantial advantages when compared to existing studies in the field. We compare it with other mainstream measurement methods in Table 3. Firstly, it stands out as a calibration-free approach, facilitating real-time monitoring of blood pressure levels over extended durations with heightened accuracy. In contrast to methodologies relying on photoplethysmography (PPG) and electrocardiogram (ECG) sensors, our method leverages ultrasonic sensors, offering a more dependable source of high-precision vascular pulse wave information for modeling data.

Moreover, in comparison to other approaches utilizing ultrasonic sensors, our method adopts a Support Vector Regression (SVR) model based on the characteristic value of the pulse wave to autonomously calibrate the parameter α. This distinctive feature contributes to the model′s enhanced accuracy, particularly during prolonged monitoring periods.

Table 3 Performance comparison with other works

Work	Signals used	Method	Calibration	Real-time ability	SBP average error (mmHg)	DBP average error (mmHg)
Our work	Ultrasound	SVR	No	2.42±2.45	0.07±4.26	
PTT&PIR [5]	ECG&PPG	PWV-formula	Yes	√	0.08±4.06	−0.18±4.13
Muti-parameter [6]	ECG&PPG	ANN	Yes	×	1.27±5.98	−1.38±5.49
Wearable ultrasonic sensor [9]	Ultrasound	Diameter-Formula	Yes	×	0.32±1.45	−1.97±2.42
Business equipment	Pressure & PPG	Direct measurement	No	×	±3	±3

*Business equipment refers to HUAWEI WatchD, which is measured by ourselves.

Limitations of this study

This study acknowledges certain limitations, primarily pertaining to participant size and the follow-up examination of long-term blood pressure measurements in larger individuals. The targeted modeling and analysis focused on hypertensive patients may result in increased errors in blood pressure prediction due to the limited sample size of this subgroup.

While this paper introduces a flexible ultrasound-based calibration-free long-term blood pressure monitoring system, contributing to the advancement of wearable ultrasound sensors and the integration of continuous blood pressure monitoring into daily life, there remain areas for further investigation and improvement:

1. Flexible ultrasound array preparation: Despite advancements, errors persist in the electrode template cutting process. Exploring the use of a more precise laser-cutting machine can further reduce fabrication errors. Additionally, the selection of flexible substrates and piezoelectric ceramic particle materials warrants deeper exploration.

2. Dataset acquisition: The sample size of the tested population remains insufficient for robust model construction. More extensive data collection is necessary, including data on human blood pressure under various abnormal conditions.

3. Model construction: The multiple linear regression and support vector machine models employed in this study exhibit limitations in parameter estimation. Enhancing predictive capabilities can be achieved by exploring neural networks or deep learning methods. The test errors for systolic and diastolic blood pressure in the final assessment were -0.24 ± 5.64 mmHg and 0.53 ± 4.92 mmHg, respectively. Notably, the systolic blood pressure error slightly exceeds 5 mmHg, indicating room for further improvement.

CONCLUSION

This paper introduces a novel approach for blood pressure measurement without a cuff. The proposed technique uses a flexible ultrasound probe-based device to estimate carotid artery blood pressure and non-invasively assess the vascular pulse wave of the radial artery at the wrist. Notably, this method enables prolonged blood pressure monitoring without the need for frequent calibration. This is achieved by extracting pulse wave characteristic values to adaptively calibrate the model's α parameters.

To evaluate the efficacy of the technique, a population test involving fifty individuals was conducted, with cuff sphygmomanometer measurements serving as reference values. The results showed a strong correlation

between the systolic blood pressure (SBP) and diastolic blood pressure (DBP) readings obtained via the proposed method and the reference values. Furthermore, 80% of the subjects exhibited blood pressure measurement errors below 8 mmHg.

The paper examines the error trends observed during long-term monitoring without calibration, highlighting the practical significance of this measurement method for sustained blood pressure tracking.

Data availability

The original data are available from corresponding authors upon reasonable request.

Acknowledgements

We appreciate the blood pressure samples and data provided by the participants for this study.

Funding

This work was supported by the National Natural Science Foundation of China (T2350001 and 52173280), the China Postdoctoral Science Foundation (2022M711256), the Huazhong University of Science and Technology (HUST) Interdisciplinary Research Project (2023JCYJ044), and the Taihu Lake Innovation Fund for Future Technology, HUST (2023A3).

Conflict of interest

J. Zang, H. Lei, Y. Yu and H. Tang are applying for a patent that covers the design of the ultrasonic device (Chinese patent, application number: 2023233958764).

Supplementary information

The supporting information is available online at https://doi.org/10.1360/nso/20240014. The supporting materials are published as submitted, without typesetting or editing. The responsibility for scientific accuracy and content remains entirely with the authors.

References

1 Krokstad S. Worldwide trends in hypertension prevalence and progress in treatment and control from 1990 to 2019: A pooled analysis of 1201 population-representative studies with 104 million participants. *Lancet* 2021; **398**: 957–980.

2 Peter L, Noury N, Cerny M. A review of methods for non-invasive and continuous blood pressure monitoring: Pulse transit time method is promising? *IRBM* 2014; **35**: 271–282.

3 Lass J, Meigas I C, Karaiet D, *et al*. Continuous blood pressure monitoring during exercise using pulse wave transit time measurement. Proc. 26th Annu. *Int Conf IEEE Eng Med Biol Soc* 2004; 2239–2242.

4 Celler BG, Le P, Basilakis J, *et al.* Improving the quality and accuracy of non-invasive blood pressure measurement by visual inspection and automated signal processing of the Korotkoff sounds. *Physiol Meas* 2017; **38**: 1006–1022.

5 Chen W, Kobayashi T, Ichikawa S, *et al.* Continuous estimation of systolic blood pressure using the pulse arrival time and intermittent calibration. *Med Biol Eng Comput* 2000; **38**: 569–574.

6 Barvik D, Cerny M, Penhaker M, *et al.* Noninvasive continuous blood pressure estimation from pulse transit time: A review of the calibration models. *IEEE Rev Biomed Eng* 2021; **15**: 138–151.

7 Nabeel PM, Karthik S, Joseph J, *et al.* Arterial blood pressure estimation from local pulse wave velocity using dual-element photoplethysmograph probe. *IEEE Trans Instrum Meas* 2018; **67**: 1399–1408.

8 Pereira T, Santos I, Oliveira T, *et al.* Characterization of optical system for hemodynamic multi-parameter assessment.

Cardiovasc Eng Tech 2013; **4**: 87–97.

9 Ding X, Zhang Y, Tsang HK, *et al*. A new modeling methodology for continuous cuffless blood pressure measurement. *IEEE EMBS Int Conf Biomed Health Inf BHI* Las Vegas, NV, USA, 2016, 264–267.

10 Fukushima H, Kawanaka H, Bhuiyan M, *et al*. Cuffless blood pressure estimation using only photoplethysmography based on cardiovascular parameters. *Proc Annu Int Conf IEEE Eng Med Biol Soc EMBS* Osaka, Japan, 2013, 2132–2135.

11 Li Y, Wang Z, Zhang L, *et al.* Characters available in photoplethysmogram for blood pressure estimation: Beyond the pulse transit time. *Australas Phys Eng Sci Med* 2014; **37**: 367–376.

12 Kim JS, Kim KK, Baek HJ, *et al.* Effect of confounding factors on blood pressure estimation using pulse arrival time. *Physiol Meas* 2008; **29**: 615–624.

13 Putyatina SY. Measurement of arterial blood pressure by processing pulse wave data. *3rd Annual Siberian Russian Workshop on Electron Devices and Materials* Altai, China, 2002, 77–78.

14 Meng K, Chen J, Li X, *et al.* Flexible weaving constructed self-powered pressure sensor enabling continuous diagnosis of cardiovascular disease and measurement of cuffless blood pressure. *Adv Funct Mater* 2019; **29**: 1806388.

15 Arndt JO, Klauske J, Mersch F. The diameter of the intact carotid artery in man. *Pflügers Archiv* 1968; **301**: 230–240.

16 Meinders JM, Hoeks APG. Simultaneous assessment of diameter and pressure waveforms in the carotid artery. *Ultrasound Med Biol* 2004; **30**: 147–154.

17 Joseph J, P M N, Shah MI, *et al.* Arterial compliance probe for cuffless evaluation of carotid pulse pressure. *PLoS One* 2018; **13**: e0202480.

18 Nissen SE, Grines CL, Gurley JC, *et al*. Application of a new phased-array ultrasound imaging catheter in the assessment of vascular dimensions. *In Vivo Comparison to Cineangiography Circulation* 1990; **81**: 660–666.

19 Huynh TH, Jafari R, Chung WY. Noninvasive cuffless blood pressure estimation using pulse transit time and impedance plethysmography. *IEEE Trans Biomed Eng* 2019; **66**: 967–976.

20 Gao M, Cheng HM, Sung SH, *et al.* Estimation of pulse transit time as a function of blood pressure using a nonlinear arterial tube-load model. *IEEE Trans Biomed Eng* 2017; **64**: 1524–1534.

21 Camasão DB, Mantovani D. The mechanical characterization of blood vessels and their substitutes in the continuous quest for physiological-relevant performances. A critical review. *Mater Today Bio* 2021; **10**: 100106.

22 Tardy Y, Meister JJ, Perret F, *et al.* Non-invasive estimate of the mechanical properties of peripheral arteries from ultrasonic and photoplethysmographic measurements. *Clin Phys Physiol Meas* 1991; **12**: 39–54.

23 Chirinos JA. Arterial stiffness: Basic concepts and measurement techniques. *J Cardiovasc Trans Res* 2012; **5**: 243–255.

24 Boutouyrie P, Fliser D, Goldsmith D, *et al.* Assessment of arterial stiffness for clinical and epidemiological studies: Methodological considerations for validation and entry into the European Renal and Cardiovascular Medicine registry. *Nephrol Dial Transplant* 2014; **29**: 232–239.